JASA ARTICLE

Optimizing the spatial extent of long-duration broadband noise signals using time reversal

Rylee S. Russell,[1] Brian E. Anderson,[1,a)] and Michael H. Denison[2]
[1]Acoustics Research Group, Department of Physics and Astronomy, Brigham Young University, Provo, Utah 84602, USA
[2]Sandia National Laboratories, Albuquerque, New Mexico 87185, USA

ABSTRACT:
The use of audible sound for acoustic excitation is commonly employed to assess and monitor structural health, as well as to replicate the acoustic environmental conditions that a structure might experience in use. Achieving the required amplitude and specified spectral shape is essential to meet industry standards. This study aims to implement a sound focusing method called time reversal (TR) to achieve higher amplitude levels compared to simply broadcasting noise. The paper seeks to understand the spatial dependence of focusing long-duration noise signals using TR to increase the spatial extent of the focus. Both one- and two-dimensional measurements are performed and analyzed using TR with noise, alongside traditional noise broadcasting without TR. The variables explored include the density of foci for a given length/area, the density of foci for varying length with a fixed number of foci, and the frequency content and bandwidth of the noise. A use case scenario is presented that utilizes a single-point focus with an upper frequency limit to maintain the desired spectral shape while achieving higher focusing amplitudes.
 https://doi.org/10.1121/10.0041760

(Received 22 April 2025; revised 28 October 2025; accepted 10 November 2025; published online 1 December 2025)
[Editor: Julien de Rosny] Pages: 4221–4234

I. INTRODUCTION

Time reversal (TR) is a method most commonly used to focus impulsive-like sounds.[1,2] Some applications that use impulsive TR include biomedical ultrasound,[1,3] communication in various media,[1,4–7] and nondestructive evaluation.[1,8,9] However, TR is not limited solely to focusing impulsive sounds. TR has been shown to effectively focus single-frequency tones,[10,11] short-duration noise,[12] and long-duration noise.[13] An application of focusing long-duration noise signals is using TR to locate non-volcanic tremor.[14] The current paper continues the study of focusing long-duration noise signals, but more specifically the spatial extent of this focusing.

Focusing long-duration noise signals follows a similar process to that of impulsive-like signals but includes an additional step. Both methods begin by obtaining an impulse response (IR). A loudspeaker placed in a room broadcasts a swept sine wave (chirp), and the response of this chirp, known as the chirp response (CR), is recorded at a location where focusing is desired that is determined by the placement of a microphone within the room. The IR is calculated using a cross-correlation method.[15] The broadcasted and recorded signals must be time-synced for the cross-correlation method to yield an IR with accurate timing when using multiple channels for TR. It is important to note that moving the loudspeaker to a different location after calculating the IR will prevent the sound waves from focusing at the original microphone location. The process up to this point will be known as the forward step. The remaining process is referred to as the backward step. Reversing the IR generates a time-reversed IR (TRIR). For impulsive focusing, broadcasting the TRIR from the same loudspeaker results in an impulsive-like focusing at the microphone. For focusing long-duration noise, an extra step is required: the TRIR is convolved with the noise signal prior to its broadcast. Broadcasting the convolved signal enables long-duration focusing through constructive interference between the direct sound waves and their reflections. Note that we define long duration such that a steady-state condition is achieved in the focusing signal, implying that the duration of the focused signal exceeds the reverberation time of the room. The use of additional loudspeakers in TR provides even higher amplitude focusing.

Certain previous studies on impulsive focusing of audible sound in rooms are considered especially relevant to the research conducted in a reverberation chamber in this paper, despite differences in their primary application. Yon *et al.*[16] showed that increasing the bandwidth and/or number of sources created a higher quality (more prominent) peak compared to the spatial sidelobes of the TR focusing. Candy *et al.*[4] demonstrated that TR transducers can effectively operate in highly reverberant environments, detecting and recovering transmitted information with zero errors. Denison and Anderson[17] concluded that decreasing the volume and absorption of a room increases the focal amplitude and quality of the focusing. Some researchers have explored high-amplitude focusing of sound in rooms,[18,19] and pipes,[20] and the nonlinear properties of that focusing. Farin *et al.*[21,22] explored TR focusing of sound to excite complex structures,

a)Email: bea@byu.edu

enabling selective excitation and damage detection without disassembly.

A study by Ribay *et al.*[12] explored the focusing of pulses and borderline long-duration noise signals. It was found that the quality of the focusing increased as the number of loudspeakers increased. Anderson *et al.*[10] found that multiple sources must be used to obtain TR spatial focusing of single-frequency tones. In Ref. 13, the focusing of long-duration noise with a desired spectrum at a single location was shown, achieving increased amplitude compared to merely broadcasting the noise. Note in Ref. 13 (their Fig. 4) that a steady-state amplitude is achieved between 2 and 7 s for the long-duration noise signal that is focused. Ribay *et al.*,[12] Anderson *et al.*,[10] and Russell *et al.*[13] each demonstrated the concept of coherent addition in their respective contributions.

Previous studies explored the spatial extent of impulsive focusing. Tanter *et al.*[23] showed that applying an inverse filter in TR focusing can reduce spatial sidelobes amplitudes. Others have also explored TR with the use of an inverse filter/deconvolution.[24,25] Yon *et al.*[16] found that increasing the number of loudspeakers used for TR focusing decreases the focus spot diameter and the relative amplitude of spatial sidelobes in free space, but that in a reverberation chamber the spot diameter depends more on the center frequency than the number of loudspeakers. Kingsley *et al.*[26] explored the spatial extent of multipoint focusing with different spatially shaped foci. By applying a spatial inverse filter, they were able to achieve dipole, quadrupoles, and "Y" shaped patterns. This technique was attempted for the present study, but it was found that the spectral content of the focused signal is significantly modified by the spatial inverse filter and thus not explored further for the present application.

Anderson *et al.*[27] conducted a study on the spatial reconstruction of pulses with a center frequency of 200 kHz using TR techniques with ultrasonic elastic waves in an aluminum plate. The experiments utilized virtual sources, starting with two foci and increasing up to 25 foci, with a constant 1-mm spacing between each source. The objective was to simulate sources spanning from a point source up to an extended line source spanning a linear distance of 1.5 wavelengths. The study evaluated several metrics: the peak magnitude of the TR focus, the ratio of the peak magnitude to the next highest spatial peak, the comparison of peak magnitude to the average wave field magnitude (excluding the main focal lobe), and the ratio of peak focal magnitude to the highest temporal sidelobe magnitude. The findings indicated that the ability to spatially reconstruct coherent sources with TR foci diminishes as the source size exceeds half a wavelength.

This paper extends the study of focusing broadband audible noise, specifically examining the spatial extent of the focus under various conditions. The purpose of this paper is to quantify how the spatial extent of TR focusing (with a single focus or multiple foci) depends on factors, such as the density of focus points for a given length/area of focusing (Sec. III A), the variation in length of focusing with a fixed number of focus points (Sec. III B), and the frequency content and bandwidth of the noise (Sec. III). The study found that adjusting the density of focus locations in either one or two dimensions affects both the overall sound pressure level (OASPL) and the shape of the desired spectrum. Constructive and destructive interference was observed most prominently between adjacent focus points, depending on their spacing and frequency. By applying an equalization step, the spectra were corrected, revealing an upper frequency limit for focusing a desired frequency bandwidth across various target areas (Sec. III C). This method produced higher spatially averaged amplitude compared to broadcasting noise signals, offering a practical solution for achieving higher-amplitude gains without distorting the spectral shape. The work by the authors in Ref. 13 centered on focusing only at one location, exploring the impact of the duration of the focused noise and exploring techniques to equalize the spectral content at the focal location to achieve the desired spectrum (summarized here in Sec. II C). Achieving required amplitudes and a specified spectral shape is essential to meet certain industry standards.[28]

II. EXPERIMENTAL DETAILS

A. Setup

Spatial measurements of sound fields were measured using a 2D scanning system at Brigham Young University. The scanning system has two controllers (Applied Motion Products STAC 6i) connected to stepper motors (Applied Motion Products HT23-550D) that control the position of a microphone mounting arm. The scanning system can move the microphone in a plane, in a $2 \times 2\,\mathrm{m}^2$ area. The scanning system is operated through a custom LabVIEW program, Easy Spectrum Time Reversal,[29] which offers various functions for facilitating TR experiments. It integrates with Spectrum M2i.6022 and M2i.4931 signal generation and digitizer cards, enabling synchronized broadcasting and recording. This synchronization is crucial for ensuring that TRIR broadcasts from multiple loudspeakers reach the focus location simultaneously to ensure precise timing.

Easy Spectrum Time Reversal can broadcast and record signals for each loudspeaker either simultaneously or sequentially at each scanning grid position with the 2D scanning system, which is set to pause at each location when recording before proceeding to the next location. This automation of the forward and backward steps is essential, particularly when the number of microphones is limited, as it allows for experiments to be conducted across multiple recording locations for a repeatable experiment in a timely manner. For the experiment to be repeatable, it is assumed the conditions of the room are not changing, such as temperature. There are some prepping steps in between the forward step and backward step for focusing long-duration noise signals discussed in Sec. II B.

The reverberation chamber has dimensions of 4.96 m $\times$ 5.89 m $\times$ 6.98 m (volume of $204\,\mathrm{m}^3$). The Schroeder

https://doi.org/10.1121/10.0041760

frequency of the chamber is 400 Hz with a reverberation time of 7.6 s.[19,30] However, the lowest frequency used across all signals in the experiments is 56 Hz, corresponding to the lowest frequency in the 63 Hz one-third octave band. Diffuser panels hang from the ceiling of the chamber, which serve to randomize the propagation directions of reflections in the sound field. To achieve higher focal amplitudes, Mackie HR824mk2 loudspeakers, placed on stands about 1 m off of the floor, were each placed facing the nearest wall about 15 cm away. This orientation was chosen to minimize the direct sound amplitude.[15] The microphone used in all experiments was a G.R.A.S. 46AQ 1.27 cm (0.5 inch) prepolarized, random-incidence microphone, which was mounted on the arm of the 2D scanning system and powered by a G.R.A.S 12AX signal conditioner. To adhere to standards for being in the diffuse field[31] and to prevent a doubling of pressure,[32] the microphone was always positioned at least 1 m away from any wall or large surface. Since the 2D plane was oriented vertically in the room (as shown in Fig. 1), the scanning grid was set to ensure it remained 1 m above the ground.

The TRIR was trimmed down to a duration of 2 s, following the guideline given by Willardson *et al.*[18] who utilized the same chamber for their experiments. The noise signal that was convolved with the TRIR was chosen to have a duration of 10 s. A steady-state amplitude was apparent after the first 2 s of the recording of the signal during TR focusing. The portion of time between 2 and 12 s was used to determine the spectral amplitudes during this long-duration steady-state focusing. Block averaging was used to quantify spectral amplitudes with a block size of 0.5 s and 50% overlap. These settings were consistent for all experiments in this paper.

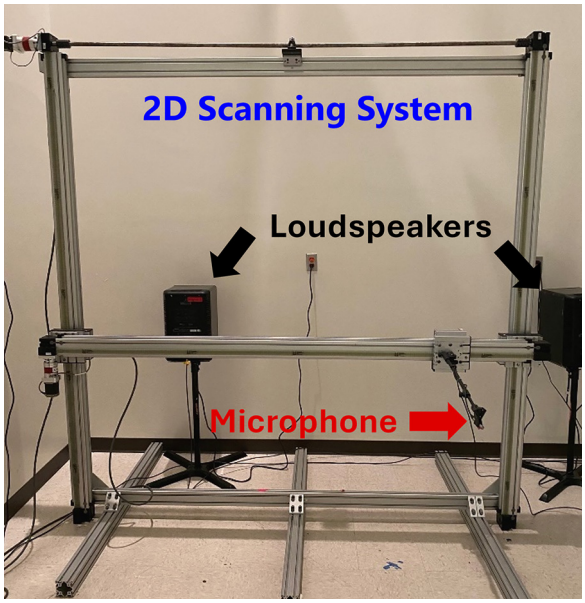

FIG. 1. Photograph of loudspeakers (black arrows) and a microphone (red arrow) mounted to the arm of the 2D scanning system placed in the reverberation chamber at Brigham Young University.

B. Multipoint TR focusing

To explore increasing the spatial extent, focusing to multiple locations will be done simultaneously. For simplicity and clarity, consider the following thought experiment with two focus locations and two loudspeakers.

The process of focusing to multiple locations begins by gathering IRs, as described in Sec. I. In this case, IRs are collected from each loudspeaker to each focal location, resulting in a total of four IRs: two IRs from each loudspeaker to the two focal points. These IRs contain the necessary timing information of sound arrivals to create a focus at each desired location. To create multiple foci, each IR, $h_{m,n}(t)$, is reversed in time to obtain the TRIR, $h_{m,n}(-t)$, with m being a source channel index and n being a focal location index.

For focusing broadband noise, we first convolve the noise signal $s(t)$ with each TRIR $h_{m,n}(-t)$,

$$cs_{m,n}(t') = h_{m,n}(-t) * s(t). \tag{1}$$

Time in the convolution result, $cs_{m,n}(t')$, is denoted by t' to recognize that the convolution result has a longer span of time than t when using discrete-time signals. Each convolved signal, $cs_{m,n}(t')$, corresponds to the signal used to focus noise at a specific location when broadcast. The next step involves broadcasting these convolved signals, which is equivalent to convolving with the original IRs, resulting in focused noise signals, $f_{m,n}(t)$, at each location:

$$f_{m,n}(t'') = cs_{m,n}(t') * h_{m,n}(t). \tag{2}$$

Here, t'' recognizes that the span of time for this convolution result is different than the time span for t' and t.

When simultaneously focusing to multiple locations, the $cs_{m,n}(t')$ signals used to focus at each focal location are added together prior to their broadcast to produce a combined broadcast signal for each respective loudspeaker. This is done by summing the n th indices of $cs_{m,n}(t')$ for each source channel, m. It is important to note that, for the signals to sum correctly, the individual signals need to be time synchronized. This ensures that focusing at both locations is done simultaneously by both loudspeakers. This approach may be generalized to any number of loudspeakers and any number of desired focal points.

If time synchronization is preserved, then the resulting focused noise signals $f_{m,n}(t'')$ generated by each loudspeaker will superpose constructively at the focal locations. This is seen by combining Eqs. (1) and (2) in the following manner:

$$f_{m,n}(t'') = h_{m,n}(-t) * s(t) * h_{m,n}(t) = R_{m,n}(t') * s(t), \tag{3}$$

where $R_{m,n}(t')$ is the autocorrelation function. Autocorrelations of broadband signals will have a large peak at $t' = 0$ with lower-level side lobes before and after. Due to this impulsive-like attribute of $R_{m,n}(t')$, the signal $f_{m,n}(t'')$ is largely correlated to $s(t)$ for all m and n. Because the IR and autocorrelations are

not perfect impulses in non-free-field environments, $f_{m,n}(t'')$ will not be an exact temporal reconstruction of $s(t)$ and thus have modified frequency content compared to $s(t)$.[23–25] Correcting for these distortions is addressed in Sec. II C.

C. Equalization process of broadcasted signals

Equalizing a convolved signal before broadcasting is crucial for achieving the desired spectrum at the focal location(s). The purpose for equalizing is to compensate for an uneven frequency response of the loudspeakers, a spatially averaged variation in gain from room modes over frequency, and frequency-dependent absorption effects during propagation. Equalization is performed in the frequency domain by taking the fast Fourier transform of the IR to obtain the transfer function, separating it into magnitude and phase components, and then modifying the magnitude while preserving the phase.

The inverse filter process addresses the magnitude disparity between the desired spectrum and the one distorted by propagation through the room twice (propagation during the forward and backward steps of TR). The half inverse filter (HIF) spectrum is used to equalize the signal to compensate for the uneven frequency response during a single broadcast step. The HIF is calculated by dividing the CR spectrum by the chirp spectrum (the complex fast Fourier transforms of these respective time signals are divided). Regularization is applied to the magnitude of the HIF spectrum to reduce high amplitudes in the HIF at inefficient transmitting frequencies, which helps avoid inefficiencies in transmission. This is achieved by dividing the HIF spectrum into one-third octave bandwidths, calculating the median amplitude for each bandwidth, and setting the amplitude of any frequencies that exceed this median equal to the median value. Tanter *et al.*[23] used single value decomposition to minimize large errors from small systemic errors during inversion. Similarly, Anderson *et al.*[25] applied regularization by adding a finite value to the inverse filter denominator, reducing background noise by preventing division by zero or small values outside the bandwidth. However, this issue of amplifying noise outside of the bandwidth is not a problem with the implementation used here because the inverse filter is applied only to the frequencies being used. The frequencies are modified only within each one-third octave band, not across the overall spectrum.

Regularization applied to the HIF spectrum results in a signal that is not dominated by frequencies that were weakly received during the forward step and thus amplified the most by an HIF without regularization. This leads to a more efficient broadcast of overall energy. To achieve a TR focal signal that has a flat spectrum, the HIF must be applied to the $cs_{m,n}(t)$ twice to compensate for the forward step propagation that has already happened and to anticipate the frequency dependence of the backward step propagation. To generate equalized noise at a location without the use of TR, the HIF is only applied once in anticipation of the single propagation step. The phase of the $cs_{m,n}(t)$ spectrum or noise spectrum is reattached after the HIF multiplications and regularization prior to performing an inverse fast Fourier transform to obtain the time domain signal to be broadcast. It is important to note that the chosen noise signal convolved with the TRIR may have any desired spectrum. Additional details on this methodology and implementation are found in Ref. 13.

III. EXPERIMENTS AND RESULTS

A. One-dimensional (1D) scans

1D multipoint focusing is now discussed. The scanning system moved horizontally without any vertical movement. All data were obtained exclusively through experimental measurements for both the forward and backward steps. The sound pressure levels are given in dB relative to 20 μPa. The two primary experiments for 1D scans explore varying the following two parameters: the density of foci within a fixed length (progressively adding more and more individual foci) and the density of foci across different lengths with a fixed number of foci (progressively spreading out the distance between all adjacent foci). White noise was used in these experiments with frequency content between the 630 Hz and 10 kHz one-third octave bands (spanning 13 one-third octave bands). This bandwidth is used here to ensure that our frequency content is above the room's Schroeder frequency, to ensure that strong modal effects do not impact the studies described in this section. The plots presented have position and frequency on the x-y plane, with amplitude measured in dB on the z axis. The frequency information displayed in the plots is not narrowband, but rather one-third octave band levels. Plotted in this way, white noise exhibits a linearly increasing trend with increasing frequency because each one-third octave band represents more energy at higher frequencies, whereas, for example, pink noise would appear as a flat line due to its equal energy distribution per octave.

For reference, Fig. 2(a) shows the results of a 1D scan of non-focused noise present at those locations that was equalized to produce a white noise spectrum. In contrast, Fig. 2(b) presents a scan of the field at those locations with a single point TR focus at the 0.75 m mark using equalized white noise. The previous study, Russell *et al.*,[13] indicated that at the focus location, both focused and non-focused noise maintain the same noise spectra, with the focused noise having a higher amplitude of roughly 3 dB gain per doubling of loudspeakers. This pattern is evident in the comparison of Figs. 2(a) and 2(b) at the focus location, although the single point focus exhibits an expected spatial width that varies with frequency. Locations away from the focus location thus have lower amplitude at all frequencies. While the increased amplitude from using TR is advantageous, the spatial extent of the focus is limited to a wavelength in size with a single focus location. However, by focusing at multiple locations, the spatial extent of the focused noise might

https://doi.org/10.1121/10.0041760

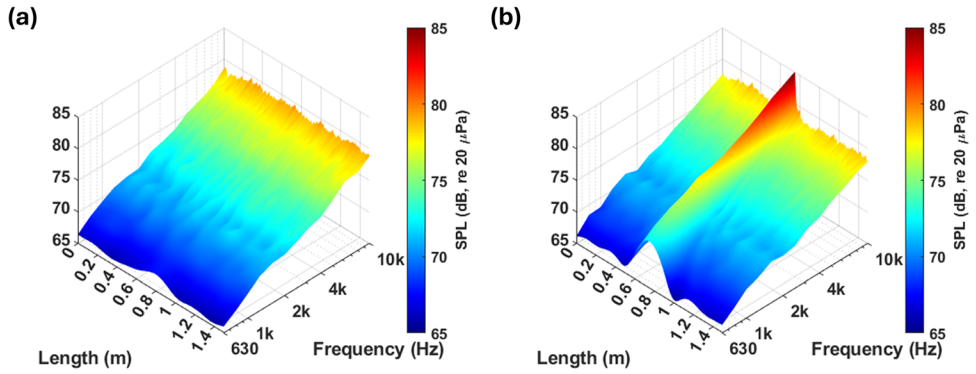

FIG. 2. 1D spatial scan of broadcasting (a) equalized noise to achieve a white noise spectrum everywhere in the reverberation chamber, and (b) focusing equalized noise to achieve a white noise spectrum at the focus location.

be extended, thereby increasing the amplitude gain from TR over a larger region.

In the first study, with results shown in Fig. 3, the density of multiple, simultaneous TR foci was varied within a fixed span length of 1.28 m, referred to as the target region, to where the focal locations were limited. To observe edge effects from the focus locations situated at the farthest left and right positions, the total scan length was extended to 1.5 m. Measurements were made every 1 cm across the scan line. The number of foci created were as follows: 1, 4, 5, 9, 17, 33, 65, and 129, all focused within the target region with equal spacing between adjacent foci.

Figure 3 shows the OASPL as a function of position along the scan line. The results indicate that it is possible to focus long-duration noise signals at multiple locations with higher amplitude than without TR focusing. Lower densities of focal locations result in more distinctive focal hot spots across the target region, which is not ideal when a spatially uniform distribution of noise is desired. As the density of foci increases,

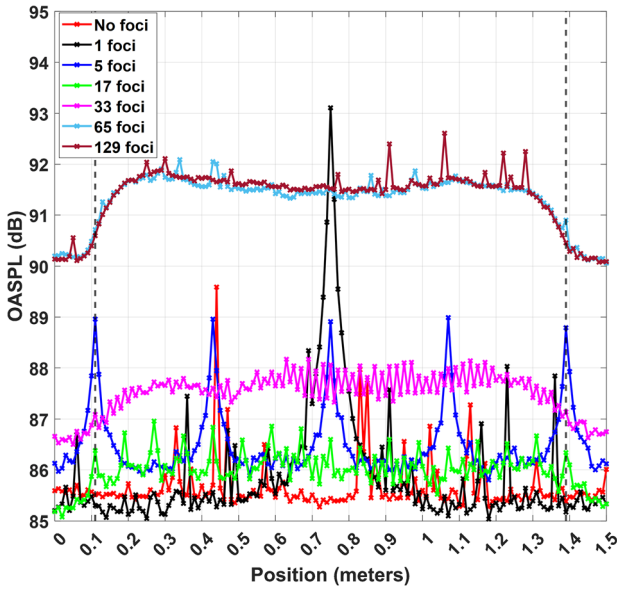

FIG. 3. OASPL as a function of position when varying numbers of TR foci are generated. Black vertical lines indicate the 1.28-m length to which the foci are confined.

the OASPL levels become more spatially uniform across the target region and larger in amplitude, compared to the pronounced spikes observed with lower numbers of foci. This spatial uniformity in OASPL and increased overall amplitude are benefits of using TR with noise, but a deeper analysis reveals that it may not be ideal in terms of frequency content. It is worth noting that, when comparing the 65 and 129 foci results, there appears to be a saturation density of points within a given length, which does not result in additional amplitude gains. Based on these data, for the given target region and frequency content, the optimal focal density appears to lie somewhere between 33 and 65 focal locations. This observation was not explored further beyond what is noted here. As for the no focusing case, when noise is played by all loudspeakers, the random spikes occur due to the combined contribution of room modes at each location, where certain areas experience greater constructive interference.

The individual focus result in Fig. 3 can be analyzed in terms of the full width at half of the maximum (FWHM) and in terms of the amplitude of the peak compared to amplitudes outside of the focal region. This analysis quantifies the spatial extent of the focusing and the spatial quality of the focusing. The FWHM is normally found by squaring the linear amplitude values, such that the squared amplitude now represents an energy quantity and then determining the width of the peak at the −6 dB down points on either side (–6 dB represents half of the maximum energy). The width in this case is 3.19 cm. The highest frequency in the bandwidth used is 11 200 Hz, which is the highest frequency in the 10 000 Hz one-third octave band. The wavelength at 11 200 Hz is 3.06 cm (assuming the speed of sound is 343 m/s); thus, the FWHM of a single TR focus peak is essentially equal to a wavelength of the highest frequency in the bandwidth (only 4% larger). The amplitude of the single TR focus peak is 93.1 dB, while the average amplitude (excluding the spikes) away from the peak is 85.5 dB, a difference of 7.6 dB, meaning the peak is 2.4 times larger than the amplitude away from the focal region.

Figures 4(a)–4(d) present the results for 5, 17, 33, and 129 simultaneous focal locations as a function of position, frequency, and level. A video link is provided in Mm. 1 to show the progression in these plots of experimental results

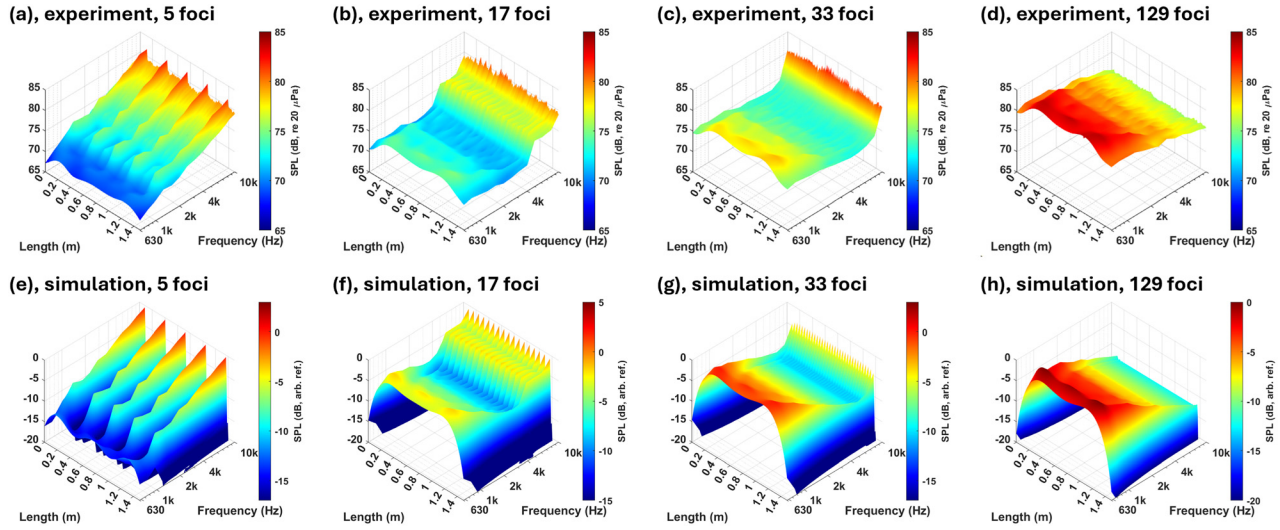

FIG. 4. Sound pressure level as a function of space and frequency (one-third octave band levels are plotted). The number of TR foci is varied while the span of the foci is kept the same: experimental results are shown in (a) 5, (b) 17, (c) 33, and (d) 129 foci, and simulation results are shown in (e) 5, (f) 17, (g) 33, and (h) 129 foci.

as the number of focal locations in increased, including results not shown in Fig. 4. Observing the plots in Figs. 4(a)–4(d), it is apparent that the different densities of focus locations affect the spectral shape. The desired spectral shape should resemble the slope in Fig. 2(a) of 3 dB/octave. This does happen for the spectra at lower focal densities, such as in Fig. 4(a). The individual ridges in Fig. 4(a) closely resemble the slope of the ridge in Fig. 2(b), but with a smaller amplitude increase for the 5 focus location ridges. Obtaining the desired spectrum of the noise is a critical desired outcome, but the spatial uniformity still remains a problem with only 5 foci. As the density of foci increases, the OASPL is more spatially uniform, as seen in Fig. 3, but higher density foci also result in spectra that depart from the spectrum of white noise.

Mm. 1. An animation of the progression as the number of focal locations increasing from 4, 5, 9, 17, 33, 65, and 129, showing plots of amplitudes as a function of space and frequency.

Analyzing Fig. 4, there is a noticeable dip in the one-third octave band levels over a small range of frequency as the density of the foci increases. The dip occurs at a frequency whose wavelength is similar to the spacing between the foci. For example, in the case of 17 foci [Fig. 4(b), and in Fig. 4(f) with simulations explained later in this section], the spacing between foci is 8 cm; and if this distance were a wavelength, it would correspond to a frequency of approximately 4.3 kHz and fall within the 4 kHz one-third octave band, where the amplitude dips. As the spacing between the foci decreases, the corresponding frequency of the dip increases. In Fig. 4(c) and in Fig. 4(g) (with simulations explained later in this section), where the foci are spaced 4 cm apart, a wavelength of this distance would correspond to a frequency of approximately 8.6 kHz falling within the 8 kHz one-third octave band, again approximately where the dip in amplitude is observed.

This dip can be explained with the use of a finding of Cassereau and Fink[33] who used the Cardinal sine, or $\mathrm{sinc}(kx) = \sin(kx)/kx$, function to model the optimal spatial extent of free-field time-reversal focusing of waves in spherical coordinates, where k is the wavenumber. The authors of the current paper verified that the spatial dependence of the focusing in all 3 dimensions is indeed a $\mathrm{sinc}(kx)$ function by placing hundreds of point sources at various angles surrounding an origin with equal radial distances. A single frequency sine wave was simultaneously broadcast from all these sources and the resultant interference near the origin was observed to indeed be a $\mathrm{sinc}(kx)$ function in any dimension for the spatial dependence. For the TR focusing to result in a $\mathrm{sinc}(kx)$ function, waves need to converge from all directions of approximately equal amplitude, and this is most likely to happen in a highly reverberant environment, such as in a reverberation chamber. A chamber or cavity with a long reverberation time results in many thousands of image sources. During the backward step of TR propagation, the emissions from the real and image sources can converge from nearly every direction (as assumed for a diffuse sound field), though generally not all with the same amplitudes without a time-dependent amplitude compensation applied (image sources further from the focal location will normally provide smaller amplitude arrival contributions to the focusing without this compensation). An enclosed cavity also results in side lobes, which are easily visible for impulsive TR focusing, and this results in propagating energy within the cavity that does not constructive interfere at the focal location; thus, it further detracts from the spatial dependence of the TR focusing being modeled as a $\mathrm{sinc}(kx)$ function. However, in the immediate vicinity of the focal location, a $\mathrm{sinc}(kx)$ function can describe the approximate spatial dependence of the TR focusing; and if the focused

https://doi.org/10.1121/10.0041760

signal is in a steady-state condition (long duration), then a sort of standing $\mathrm{sinc}(kx)$ wave is observed [the magnitude over time maintains this $\mathrm{sinc}(kx)$ shape] at the TR focus location for each frequency. When exciting a room at a single excitation frequency, there are contributions from many room modes (whose natural frequencies are nearby the excitation frequency) that are summed, since the bandwidth of each mode is finite for a room with a finite amount of damping; thus, the authors believe that TR focusing at each frequency locally provides a spatial dependence that has a $\mathrm{sinc}(kx)$ shape, as will be demonstrated.

$A\mathrm{sinc}(kx)e^{j(\omega t+\phi)}$ functions were created for every frequency, ω, in the bandwidth, with a 1-Hz spacing. For each function, the initial phase, ϕ, was randomly chosen and the magnitude, A, matched that which was used experimentally. All functions were then summed. The peaks of these $\mathrm{sinc}(kx)$ functions were then placed at the same foci locations as those used experimentally in Figs. 4(a)–4(d). These "simulation" results are included in Figs. 4(e)–4(h). The top row of plots in Fig. 4 are experimental results while the bottom row are corresponding simulation results. Good qualitative agreement between experimental and simulation results of TR focusing at multiple locations can be observed, particularly along the frequency dimension. Importantly, there are dips in the results of each type at the same frequencies for respective numbers of foci. This comparison demonstrated that using $\mathrm{sinc}(kx)$ functions to model TR focusing of steady-state, long-duration signals is useful for qualitative understanding of what the sound field can be expected to look like. There are differences, with sharper drop offs in amplitude as you spatially move away from a focal location. The authors did explore artificially adding white noise of equal amplitude at every location to improve the agreement of the simulation results with the experimental results; and while this proved to be effective, it was not immediately obvious how to predict what levels of noise needed to be added to yield the best agreement. When standing $\mathrm{sinc}(kx)$ functions are added with the same amplitudes at each frequency within the bandwidth, it produces a peak that has a FWHM of 1.11 times the wavelength of the highest frequency included. This finding is similar to the FWHM that was found for a single experimental focus, with that FWHM being 1.04 times the wavelength of the highest frequency included.

Figure 5 illustrates two standing $\mathrm{sinc}(kx)$ functions located a distance d apart. These figures show the interaction of three arbitrary frequencies in the spatial domain, highlighting how $\mathrm{sinc}(kx)$ standing waves influence wave focusing. In Fig. 5(a), when lower-frequency foci are closely spaced, the main lobes at the two focal points interact constructively, reinforcing each other. The maximum constructive interference possible, occurring when they focus at the same location, is a 6-dB gain. In contrast, Fig. 5(b) shows that, if the standing waves are spaced so that the mainlobe of one aligns perfectly with the deepest trough of the other, it results in destructive interference at each of the two focal points for that frequency. The expected amount of destructive interference for Fig. 5(b) is a 2.1-dB reduction of each focal peak. This derives from taking the difference in amplitudes between the peak (amplitude value of 1) and the trough amplitude of the sidelobe (–0.217) of the other focus resulting in a peak of only 0.783 and comparing it to an amplitude of 1.0 as a dB value. Adding a third focus location spaced the same distance away would double that amplitude decrease for the middle focus location to a 4.3-dB reduction with appropriate rounding. The frequency that results in this maximal destructive inference (the frequency of the dip), f_d, is as follows:

$$f_d = 0.715\frac{c}{d}, \tag{4}$$

where c is the speed of sound. The constant 0.715 derives from the location of the largest trough of the $\mathrm{sinc}(kx)$ function relative to a wavelength. Finally, Fig. 5(c) demonstrates that, when the focal points are sufficiently spaced apart relative to a wavelength, there is minimal interference between the two foci; this allows the standing waves to essentially behave independently, with little interaction between them.

When standing $\mathrm{sinc}(kx)$ waves interfere with each other, it results in the deviation of the spectrum from the target spectrum (white noise); this is further demonstrated in the next study. The goal of this study is to explore the effect of changing the span of foci while keeping the number of foci fixed. Figure 6 presents results where each case has 11

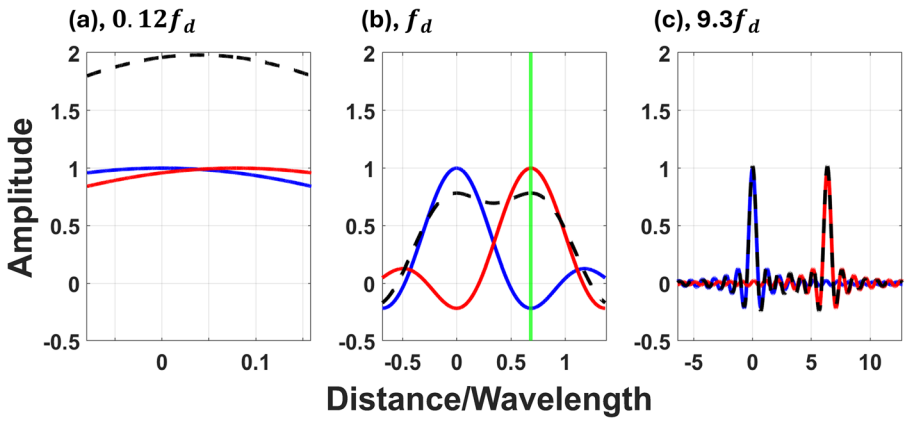

FIG. 5. Interaction of standing sinc(kx) functions located a scaled distance of $0.715\frac{c}{f_d}$ apart at three frequencies. (a) Close spacing leads to constructive interference. (b) Alignment of a peak with a trough causes destructive interference. (c) Sufficient spacing minimizes interference, allowing independent wave behavior at a frequency $9.3f_d$. The black dashed line indicates the summed results between the two standing waves in each plot.

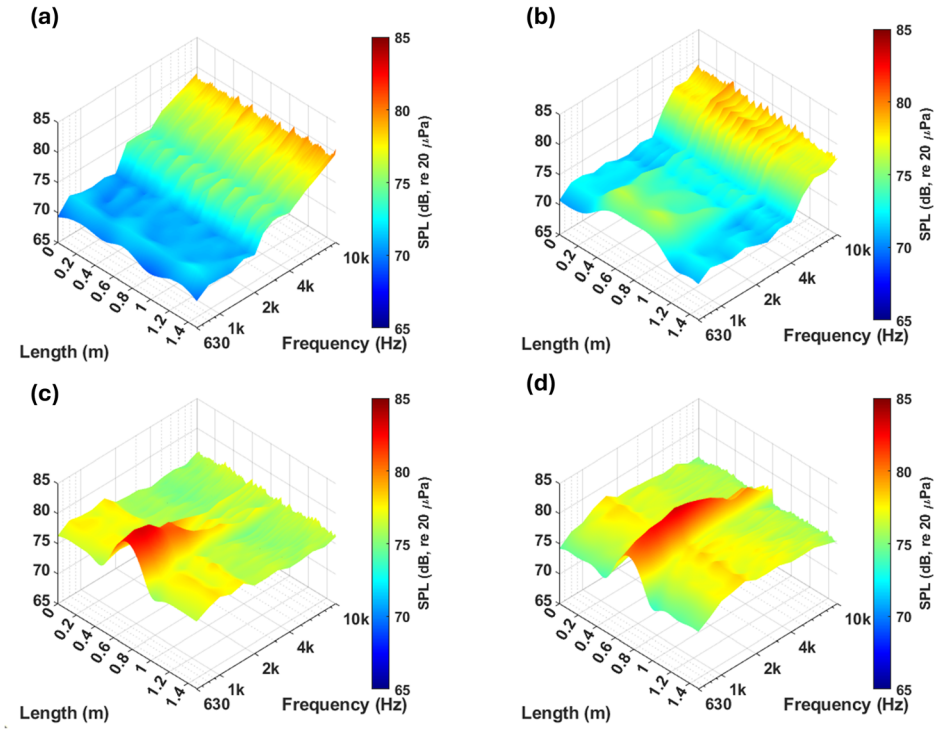

FIG. 6. Sound pressure level as a function of space and frequency, plotted as one-third octave levels. This second study explores the effect of changing the density of foci across different span lengths while keeping the number of foci fixed at 11. The scanning grid covers 1.5 m, with the span of foci changing from (a) 150 cm, (b) 75 cm, (c) 30 cm, to (d) 10 cm spacing.

foci, with equal spacing between adjacent foci for each result. The foci are always centered around the 0.75-m mark for all span lengths. The span lengths explored are as follows: 150, 135, 120, 105, 90, 75, 60, 45, 35, 30, 20, 15, 10, and 5 cm, and a single-point focus (results are shown in Fig. 6 for 150, 75, 30, 10 cm). The other results are visible in an animation that progressively shows the results, which is shown in Mm. 2.

Mm. 2. Animation of the progression as the span of a fixed number of focal locations decreases from 150, 135, 120, 105, 90, 75, 60, 45, 35, 30, 20, 15, 10, and 5 cm, and a single-point focus.

From Figs. 6(a) and 6(b), the 630- to 1600-Hz one-third octave band levels increased in amplitude due to constructive interference, as the span length decreased from 150 to 75 cm. This constructive interference, when the wavelength is larger than the spacing, occurred at progressively higher frequencies as the span length decreased. The 2500- to 4000-Hz one-third octave band levels from, again, Figs. 6(a) and 6(b) exhibit the dip in amplitude, reflecting a situation more akin to Fig. 5(b). Beyond the 4000-Hz one-third band moving from Fig. 6(a) to Fig. 6(b) in Fig. 6, the amplitude levels at these frequencies seem unaffected by interference from other foci, like the scenario depicted in Fig. 5(c). As the span length and thus spacing between each foci decrease further, as in Fig. 6(c), the amplitudes at lower frequencies begin to increase in a relative sense, while the amplitudes at frequencies above the 2000-Hz one-third octave band are lower in level than desired. Finally, in Fig. 6(d), the amplitudes at nearly all frequencies begin to constructively interfere with each other essentially as a single point focus. The animation (Mm. 2) illustrates the progressive changes as the spacing of foci becomes favorable, unfavorable, or neither in relation to the amplitude changes for each frequency band. It is apparent that the only scenario that does not significantly alter the desired frequency spectrum is the single point focus. This idea will continue to be discussed and analyzed in Sec. III B.

When performing the TR backward step for these second study results, a spacing of 1 cm between spatial measurement locations is maintained for every scan. However, in one experiment involving a 5-cm span length of foci, the spacing between each focus location needed to be smaller than 1 cm. To create this spacing of foci of only 0.5 cm within the 5 cm target span length, the IRs were collected at the proper 0.5-cm spacing in the forward step, but the spatial measurement sampling during the scan of the TR backward step was maintained at a spatial resolution of 1 cm.

B. 2D scans

Increasing the spatial extent of multipoint focusing in 2D is now discussed. For this study, the scanning system is moved both horizontally and vertically to experimentally collect data from a 2D grid of CRs for 8 loudspeakers. This grid of CR data is then converted to a grid of IR signals using cross-correlations. The grid of IR signals is used to simulate the spatial dependence of various TR backward step configurations. Here, again, the broadcast signals are noise signals with a desired spectrum convolved with equalized TRIRs. The backward step propagation was simulated in MATLAB, by convolving each of the 8 broadcast signals (one for each loudspeaker) with the corresponding IR at

https://doi.org/10.1121/10.0041760

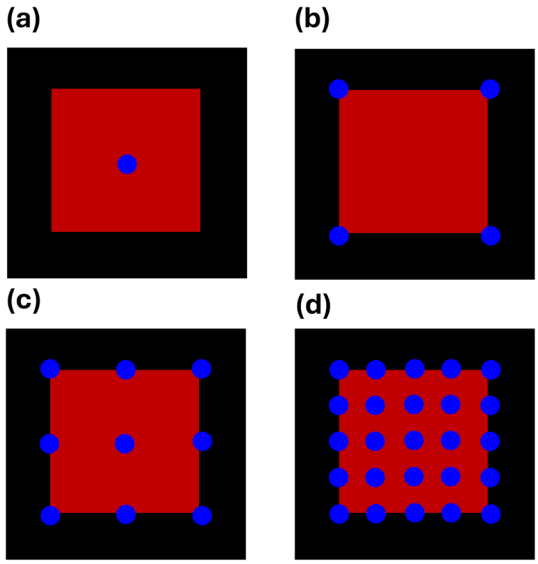

FIG. 7. The scanning grid (48 cm × 48 cm, black) and target region (24 cm × 24 cm, red) for a 2D configuration of foci. Blue dots indicate focus locations (1, 4, 9, 25) with equal spacing between adjacent foci.

every grid location. The convolved time signals corresponding to each loudspeaker broadcast were summed, essentially creating a single, cumulative recording, to produce the dataset used for analysis. In this study, since the backward step was simulated, the amplitude scale is relative and the absolute levels attained lack physical meaning, although relative differences in level can still be observed and learned from. The initial analysis includes one experiment for 2D scans that vary the density of foci within a given target region. White noise, with frequency content ranging from the 63-Hz to 10-kHz one-third octave band frequencies (spanning 23 one-third octave bands), was consistently used in all experiments for the initial analysis. Note that this expanded frequency range, particularly the additional use of lower frequencies, including below the room's Schroeder frequency, is used here for practical reasons. The intended application desires to use this full-frequency range. The authors are unaware of research that specifically explores any degradation in performance of TR techniques below the Schroeder frequency, where the room is less likely to behave as a diffuse sound field and room modes can have a stronger impact. Thus, the performance of TR within the frequency range of 56–400 Hz, below the Schroeder frequency, may be impacted more strongly by room modes. However, the authors did not observe any strong changes in the performance of TR below 400 Hz.

Shown in Fig. 7, the total size of the scanning grid is 48 cm × 48 cm (the black colored region) and the target region for the following set of experiments is 24 cm × 24 cm (the red colored region). The blue dots represent the focal location configurations, which include 1, 4, 9, 25, and 169 foci. Many more focal configurations within the target region could have been chosen, but the ones studied here are configured to have equal spacing between adjacent foci in a square lattice of foci.

For ease of interpretation, the amplitude values in the plots of this section have been adjusted by scaling them according to the bandwidth of each corresponding one-third octave band. Instead of using the standard one-third octave scaling, each frequency band's amplitude is divided by its bandwidth. This adjustment would result in a flat spectrum for white noise. The frequency axis will still display data points corresponding to the one-third octave band center frequencies. Unless otherwise specified, this scaling approach will be used throughout the remainder of this paper.

The first metric explored quantifies relative amplitude gains over the spatial extent of the 2D target region in terms of a spatially averaged amplitude for each focal configuration. For each spatial location within the target region, the one-third octave band levels were calculated and scaled. The spatially averaged amplitude was then computed for each frequency across the target region. Figure 8(a) presents the spatially averaged amplitude for seven focal configurations of focusing white noise within the target region, overlaid with the result for broadcasting equalized white noise without TR from the same number of loudspeakers. As the number of foci increases, the lower frequency content shows a noticeable increase in amplitude, while higher frequency content may perform worse than simply broadcasting white noise without TR. It is again noted that the desired outcome is a flat spectrum (white noise).

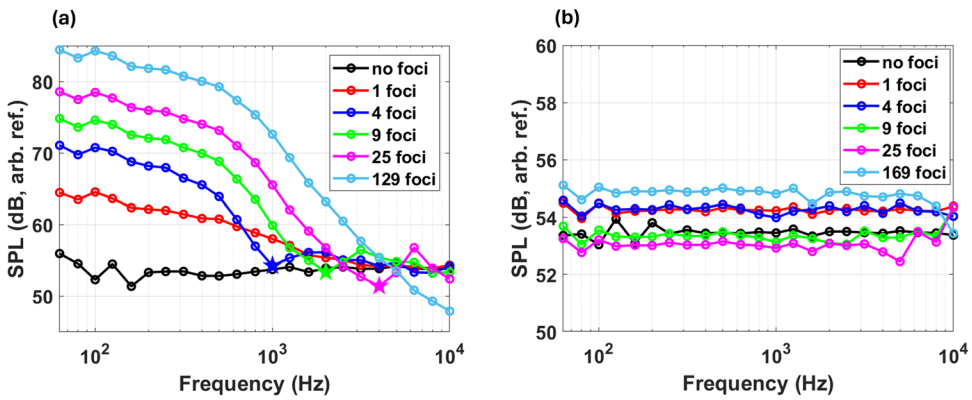

FIG. 8. (a) Spatially averaged amplitudes across the target region for different focal configurations along with a non-focusing scenario (a) while not accounting for sinc(kx) interference and (b) when accounting for the sinc(kx) interference.

The problem is that the sinc(kx) interference, discussed in Sec. III.A, is not being accounted for in the equalization for the TR focal configurations. It is important to emphasize that these plots represent spatially averaged amplitude, which explains the observed decrease in amplitude as frequency increases. Higher frequencies produce a narrower foci spatially, resulting in a lower spatially averaged amplitude compared to lower frequencies that have a larger focal width due to their longer wavelength. Adjusting the target region size would also impact the spatially averaged amplitude results: a smaller target area would result in higher frequencies averaging to a higher amplitude. Using Eq. (4), the calculated frequencies at which 4, 9, 25, and 169 foci have sinc(kx) dip interference are as follows: 1021, 2044, 4087, and 12 262 Hz, respectively. These dips are each denoted by a star in Fig. 8(a), except for the 169 foci configuration due to the sinc(kx) interference dip happening at a frequency outside of the bandwidth.

The sinc(kx) interference dip could be addressed by calculating the difference between the desired spectra and the initially obtained averaged spectra, which did not account for the interference. This correction is applied now in MATLAB by adjusting all the "broadcast signals" using the calculated difference (adjusting the already equalized signals further by equalizing to correct for the interference dip). The experiment is then repeated with the necessary equalizations to obtain the desired spectra. Figure 8(b) presents the spatially averaged amplitude for the properly equalized signals across various focus configurations. It is evident that the amplitude gains have now significantly decreased for every configuration, with the maximum achievable gain being roughly only 2 dB when compared to broadcasting white noise. The decrease in gains is a consequence of normalizing the signals to be broadcast from each loudspeaker by their peak values to maximize the input signal amplitude sent to each loudspeaker, thus resulting in a quasi-conservation of energy trade-off. Taking into account for the interference dip in the equalization eliminates the gains that are hoped for by using multipoint focusing with TR.

Figure 9 provides a different perspective on understanding the sinc(kx) interference correction through calculation of the OASPL for each spatial location in the grid. Figures 9(a) and 9(b) show the OASPL across the full 2D grid for 9 focal locations, both with and without equalization for sinc(kx) interference, while Figs. 9(c) and 9(d) present the same comparison for 4 focal locations. Without the sinc(kx) interference correction, the OASPL levels appear more rounded, with small spikes protruding slightly. However, when the sinc(kx) interference correction is applied, these spikes become more pronounced. This is expected, as without the correction, lower frequencies dominate the space while higher frequencies are reduced. By applying the correction, the higher frequencies are balanced with the lower frequencies, resulting in the correct spectral shape, but at the expense of the pronounced spikes that result from high frequency content that have a smaller spatial extent of their focusing. The pronounced spikes indicate that the target region does not have a spatially uniform distribution.

While correcting the sinc(kx) interference successfully achieves the desired spectrum over the target region, the downside is that the amplitude gain remains minimal, and

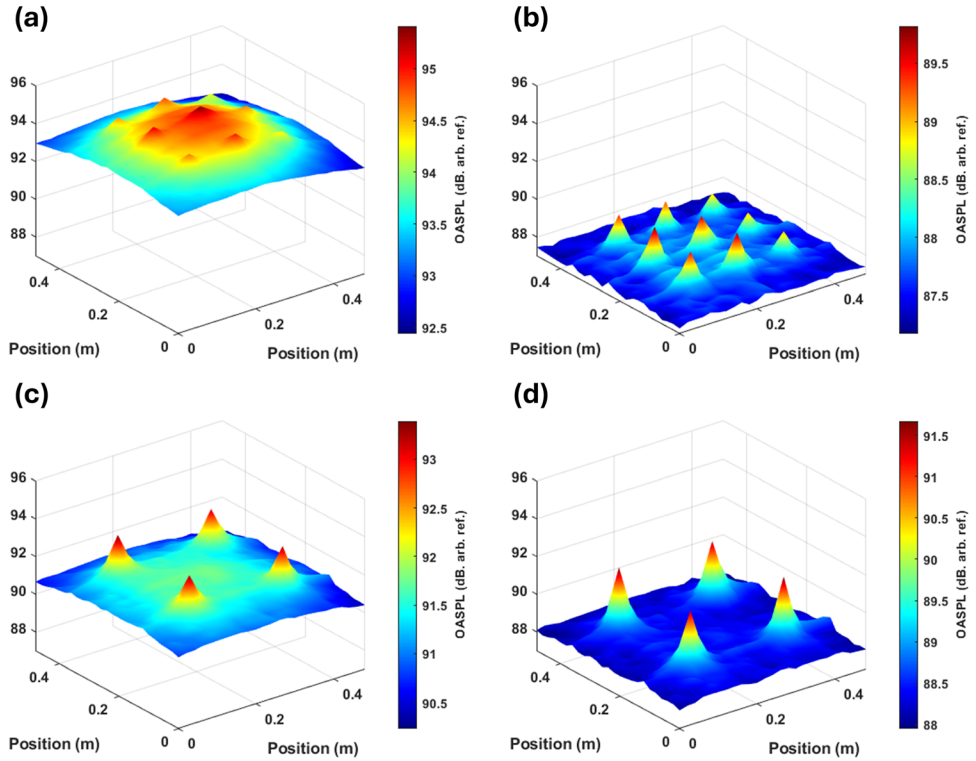

FIG. 9. OASPL distribution across a 2D grid for different multi-focusing scenarios, comparing results with [(b), (d)] and without [(a), (c)] sinc(kx) interference correction. (a), (b) The OASPL for 9 focus locations. (c), (d) Results for 4 focus locations.

https://doi.org/10.1121/10.0041760

the spatially uniform excitation is compromised. This is an apparent inevitable trade-off that cannot be avoided. To effectively compensate for the $\mathrm{sinc}(kx)$ interference while preserving the amplitude gains from TR, maintaining a spatially uniform excitation, and achieving the desired spectral shape, a different metric must be considered.

The next metric assesses the spatial variation (rather than the sum over space) within the spatial region of interest (target region) for the case of focusing noise with TR. It is desirable, for the intended use case, to have the amplitudes over all of the target region be within 3 dB of the maximum value. To start off, for each frequency band, the one-third octave band levels over the target region are normalized by setting the maximum value to 0 dB. The percentage of values among the target region that are within 3 dB of the maximum level is determined, which provides a measure of the variation in level over space. This percentage is computed for each one-third octave band frequency and focal configuration, allowing for a comparison of the spatial variation of sound energy across various focusing scenarios.

Figure 10 illustrates the spatial variation percentage across different focusing scenarios. In every scenario (including "no foci"), the same number of loudspeakers is used. While it may not be immediately apparent which scenario performs best, some trends can be observed from the plot. Notably, all focusing scenarios show that 100% of the target region falls within the -3-dB tolerance up to the 400-Hz one-third octave band. Above 400 Hz, the spatial variation of the single focus drops off, as expected, due to the narrowing of the mainlobe of the standing $\mathrm{sinc}(kx)$ wave at higher frequencies. The other multi-point focusing variations seem less predictable, but the results can be attributed to the interference patterns of the individual $\mathrm{sinc}(kx)$ standing waves at each focus location. One particular focus variation, the 4-focus scenario, manages to maintain 100% of the target region within the -3-dB range up to the 800-Hz band. This observation was noted but not explored further. Given that significant spatial variations exist above 400 Hz, there seems to be little benefit in attempting to focus frequencies above 400 Hz for this target region.

The average spatial amplitude for focusing white noise with a bandwidth of 63- to 400-Hz one-third octave frequency bands was determined. It is important to note that the expected $\mathrm{sinc}(kx)$ interference is accounted for in this case, whereas it was not accounted for in the results in Fig. 8(a). Each focus configuration was directly compared to the baseline results obtained from broadcasting white noise without TR across the same bandwidth. This ensures that all configurations were assessed relative to the broadcast of white noise without TR under equivalent conditions, allowing for consistent comparison across all configurations. As shown in Fig. 11, the findings reveal a significant amplitude gain of at least 9 dB across all frequency bands for the focus configurations, compared to broadcasting white noise from the same number of loudspeakers. In contrast, for the broader 63- to 10-kHz bandwidth in this target region [shown in Fig. 8(b)], the previously observed maximum amplitude gain was only 2 dB. The only variable change between these scenarios [Fig. 8(a) vs Fig. 11] was the decrease in bandwidth, which aligns with earlier findings in the spatial variation analysis. By not broadcasting the frequencies above the 400-Hz band, there is a corresponding apparent gain for the lower frequencies for the no TR case and an even greater gain for the TR cases [note the increase in the average levels shown in Fig. 11 versus those in Fig. 8(a)]. It is important to stress that the reduction in bandwidth impacts some of the TR focal configurations more than others. Interestingly, all TR focus configurations produced very similar level outcomes. Based on this information, it is recommended that using a single-point focus under the current conditions is just as effective as any of the other focus configurations. The current conditions refer to the specific target area and bandwidth. Section III C will provide a detailed explanation of

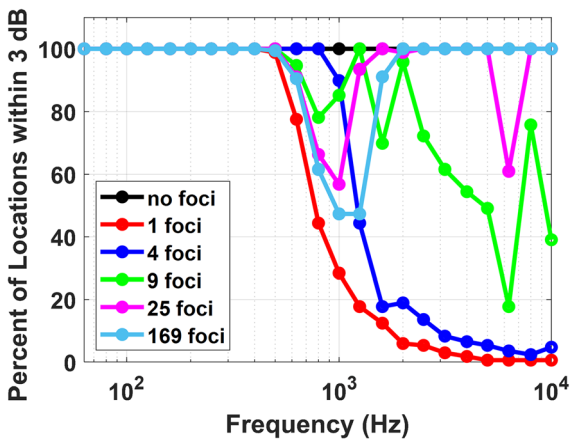

FIG. 10. Spatial variation analysis within the 2D target region (24 cm × 24 cm) for different 2D focusing scenarios (1, 4, 9, 16, 25, 49, 169 focus points). For each frequency band, the spectral data are normalized by setting the maximum amplitude to zero, and the percentage of values that deviate by more than −3 dB of the peak value within the focus region is calculated.

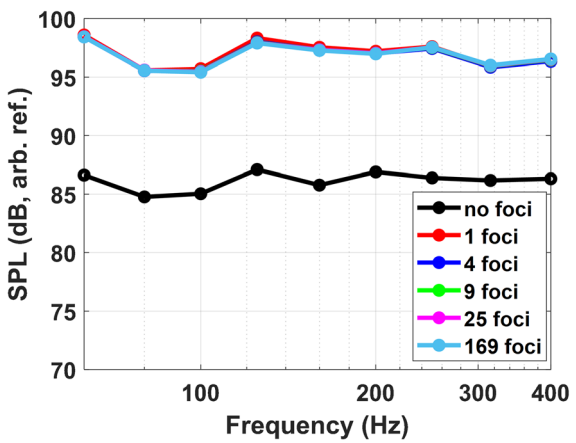

FIG. 11. Average spatial amplitude within the target region (24 cm × 24 cm) for a one-third octave frequency bandwidth from 63 to 400 Hz, while also accounting for $\mathrm{sinc}(kx)$ interference for various TR foci configurations compared to not using TR. The arbitrary dB reference in Fig. 8 was also used in this figure.

how to achieve these amplitude gains of over 9 dB for a use case scenario.

C. Use case of TR with long-duration noise signals

Using TR to focus noise for a use case scenario to achieve maximum gains, maximal spatial uniformity, and maintaining the desired spectral shape will now be discussed. A single TR focus location only will be explored due to the finding that an unavoidable trade-off exists when focusing at multiple locations in that spatial uniformity cannot be achieved simultaneously with the desired spectral shape, all while still achieving gains in amplitude due to using TR. Fortunately, the use of a single focal location helps simplify the processing by decreasing the required measurements of IRs to be made up front. The need to only measure a single IR per loudspeaker is significant in terms of reducing the amount of equipment needed from a practical standpoint. The first thing that needs to be considered is the target area. The target area, which in some cases is the size of the structure to be acoustically excited, is what ends up directly determining the usable bandwidth that can be used to focus noise with TR and achieve maximum efficiency and spatial uniformity. Lower frequencies have a larger main lobewidth for their corresponding standing $\mathrm{sinc}(kx)$ wave. The standing $\mathrm{sinc}(kx)$ wave model can be used to help determine the highest usable frequency for a specific target area. The goal is to identify the distance away from the peak at which the $\mathrm{sinc}(kx)$ function is greater than 0.707 (3 dB down from the peak) for each frequency, which will be referred to as the maximum target area radius, shown in Fig. 12. This can also be thought of as half of the FWHM distance for the squared $\mathrm{sinc}(kx)$ function (meaning the diameter is the FWHM), meaning it is inversely proportional to frequency. Figure 12 can be used to find the highest usable frequency for a specific target area that allows TR to focus noise with maximum efficiency and have the spatial distribution of amplitudes stay within –3 dB from the peak value. The maximum target area radius, r_t, shown in Fig. 12, is inversely proportional to frequency, f, and approximately equal to one-fourth of a wavelength, λ, of the highest frequency of interest, with the empirical form as follows:

$$r_t = 0.2215\frac{c}{f} = 0.2215\lambda. \tag{5}$$

In Fig. 13, the red square represents the target area of 24 cm × 24 cm discussed earlier. To determine the distance from the center of this area to its corner, we applied the Pythagorean theorem; this distance is depicted by the black line in the figure. The blue circle illustrates the size of the 2D Cardinal sine standing wave's mainlobe that remains above the −3-dB threshold. The calculated distance of 0.17 m determines the highest frequency that can be used in the bandwidth to maintain spatial uniformity to be 447 Hz (using Fig. 12), which is contained within the 400-Hz one-third octave frequency band. If frequencies are used above 447 Hz, it will result in amplitudes being more than 3 dB down from the peak, resulting in undesirable spatial variation in the target area. The bandwidth of frequencies used can be increased while maintaining the desired spatial uniformity, but the target area must be decreased according to the guidelines in Fig. 12.

Focusing noise to different target areas using a single focus location is now examined. The target areas considered include 8 cm × 8 cm, 12 cm × 12 cm, 24 cm × 24 cm, and 32 cm × 32 cm with maximum distances from the center measuring 5.7, 8.5, 11.3, and 22.6 cm, respectively. The noise band begins with the 63-Hz one-third octave band

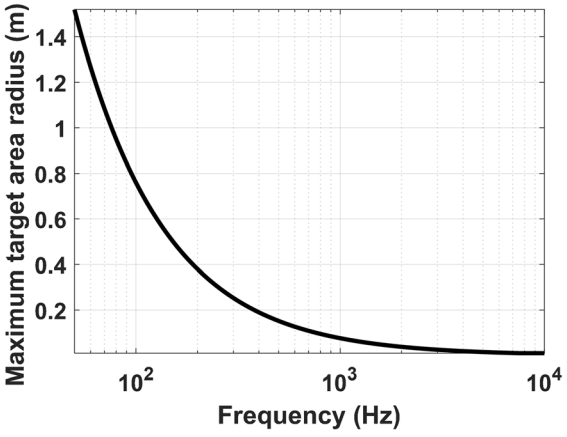

FIG. 12. The plot illustrates the trade-off between the size of the optimal target area for single point TR focusing versus the frequency upper limit of the bandwidth of frequencies that will have optimal spatial uniformity over the target region. The $\mathrm{sinc}(kx)$ function width is computed for a range of distances (0.01–1.6 m).

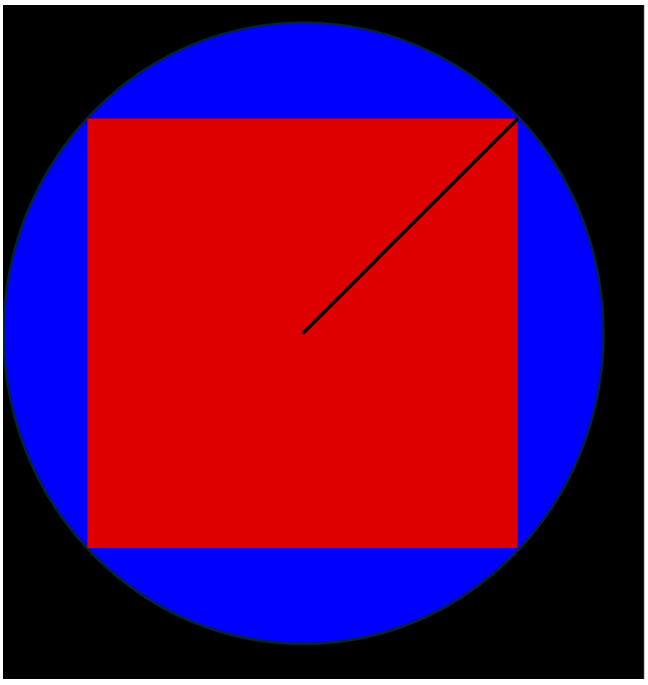

FIG. 13. The red square represents the 24 cm × 24 cm target area, with the blue circle showing the area of the highest frequency 2D Cardinal sine standing wave that is above the –3 dB threshold. The black line indicates the distance from the center to the corner of the target area, which is used to identify the highest usable frequency.

https://doi.org/10.1121/10.0041760

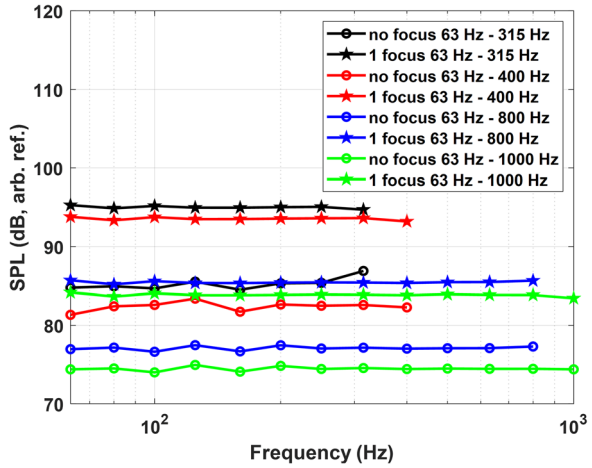

FIG. 14. Focusing noise with TR (data with star markers) compared to broadcasting noise without TR (data with circle markers). Average spatial amplitude results for different target areas, each using their respective optimal bandwidths to focus white noise. The target areas considered are (black) 32 cm × 32 cm, (red) 24 cm × 24 cm, (blue) 12 cm × 12 cm, and (green) 8 cm × 8 cm. The arbitrary dB reference in Fig. 8 was also used in this figure.

frequencies, and the upper frequency limit is determined by the maximum distance from the center of each target area, which can be determined using Fig. 12. The corresponding final one-third octave band center frequencies for these distances are 1000, 800, 400, and 315 Hz, respectively. Notably, as the target area decreases, higher frequency content can be effectively focused with maximum amplitude gains while maintaining spatial uniformity and the desired spectral shape. Figure 14 presents the average spatial amplitude results for the different target regions, using their respective bandwidths to focus white noise. The results in Fig. 14 demonstrate a minimum 9-dB increase in amplitude when focusing white noise with TR compared to broadcasting white noise without TR across all target areas (in all cases shown in Figs. 14 and 15, the same number of loudspeakers were used).

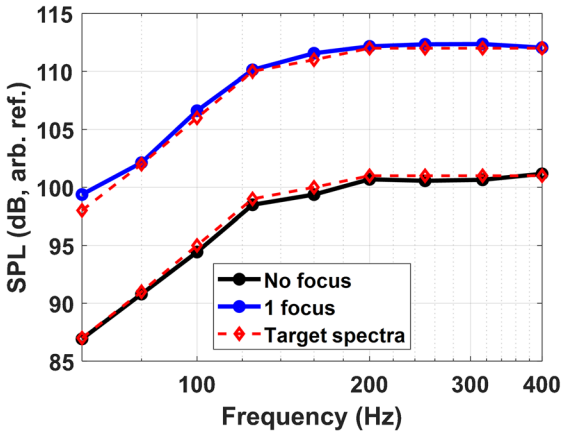

FIG. 15. Average spatial amplitude of a single TR focus of noise (blue) having the spectral shape as defined by a standard compared to not using TR (black). The green curve represents the shape of the desired spectrum, whose amplitude is scaled to fit both cases to facilitate comparison of the desired spectral shape to the resulting spectral shapes.

So far, only white noise has been considered. To expand the analysis, a spectrum specified in a standard[28] shown in Fig. 15, represented by red-colored diamond markers, was used with the same focusing process applied to white noise. This test was conducted using one of the previous target areas, specifically 24 cm × 24 cm. Given the target area, the frequency band used was 63 to 400 Hz in one-third octave frequency bands. The results in Fig. 15 show that it is possible to focus different shaped spectra of noise and still achieve significant amplitude gains when using TR compared to not using TR. The spectra shown in Fig. 15 are on a one-third octave frequency band scale that are not scaled by its corresponding band.

IV. CONCLUSION

This study investigated the spatial extent of TR focusing for long-duration broadband noise signals by varying the density of focal points and measuring their effects on OASPL and spectral shape when focusing in a line along 1D. The results showed that higher focal densities produced more uniform OASPL distributions, while lower densities led to distinct peaks. However, in the frequency domain, lower focal densities achieved the desired spectral shape but with uneven OASPL spatial distribution, while higher densities provided more uniform OASPL spatial coverage but deviated more from the desired noise spectrum. These deviations seem to result from standing $\mathrm{sinc}(kx)$ waves at each focus location that interfere with adjacent foci, which distorted the intended spectra. Similar issues arose in 2D multi-focusing experiments, regardless of focal variation (changing the density) within the intended target area. Application of an additional equalization step, used to remove the effects of $\mathrm{sinc}(kx)$ interference, corrected the spectra but also resulted in larger deviations in levels spatially across the target spatial region. Here, we explored focusing noise within a reverberation chamber with a sound field that can be considered a diffuse field, further modeling or simulations may be useful for understanding the key influential properties of focusing noise within a room that cannot be considered to have a diffuse field.

It was determined that, if a single TR focus is created and the bandwidth is limited, the spatial variations can be minimized over a known area with a radius of approximately one-fourth of a wavelength for the highest frequency in the bandwidth. Within this minimized bandwidth, TR provided a 9-dB gain over not using TR, and it was also shown that it is possible to preserve the desired spectral shape and spatial uniformity in the TR focusing. For practical applications, a single-point focus with an upper frequency limit (determined by the desired target area) can achieve equivalent amplitude gains to multi-focus configurations. This approach is practically advantageous because it simplifies the process by requiring only one IR per loudspeaker, rather than multiple IRs per loudspeaker. The target area dictates an upper frequency limit, as it is desired to maintain amplitudes within this area to be no less than

–3 dB from the maximum value, reducing spatial variation, while also maintaining the desired spectrum.

ACKNOWLEDGMENTS

This work was supported by Sandia National Laboratory No. 2346802. Sandia National Laboratories is a multi-mission laboratory managed and operated by National Technology & Engineering Solutions of Sandia, LLC (NTESS), a wholly owned subsidiary of Honeywell International Inc., for the U.S. Department of Energy's National Nuclear Security Administration under Contract No. DE-NA0003525. This written work is authored by an employee of NTESS. The employee, not NTESS, owns the right, title, and interest in and to the written work and is responsible for its contents. Any subjective views or opinions that might be expressed in the written work do not necessarily represent the views of the U.S. government. The publisher acknowledges that the U.S. government retains a non-exclusive, paid-up, irrevocable, world-wide license to publish or reproduce the published form of this written work or allow others to do so, for U.S. government purposes. The Department of Energy will provide public access to results of federally sponsored research in accordance with the Department of Energy Public Access Plan.

AUTHOR DECLARATIONS

Conflict of Interest

The authors have no conflicts to disclose

DATA AVAILABILITY

The data that support the findings of this study are available from the corresponding author upon reasonable request.

[1]M. Fink, "Time reversed acoustics," Phys. Today **50**(3), 34–40 (1997).
[2]B. E. Anderson, M. Griffa, C. Larmat, T. J. Ulrich, and P. A. Johnson, "Time reversal," Acoust. Today **4**(1), 5–16 (2008).
[3]M. Fink, G. Montaldo, and M. Tanter, "Time-reversal acoustics in biomedical engineering," Annu. Rev. Biomed. Eng. **5**, 465–497 (2003).
[4]J. V. Candy, A. W. Meyer, A. J. Poggio, and B. L. Guidry, "Time reversal processing for an acoustic communications experiment in a highly reverberant environment," J. Acoust. Soc. Am. **115**(4), 1621–1631 (2004).
[5]C. S. Clay and B. E. Anderson, "Matched signals: The beginnings of time reversal," Proc. Mtgs. Acoust. **12**(1), 055001 (2011).
[6]B. E. Anderson, T. J. Ulrich, P.-Y. Le Bas, and J. A. Ten Cate, "Three dimensional time reversal communications in elastic media," J. Acoust. Soc. Am. **139**(2), EL25–EL30 (2016).
[7]C. Song, "An overview of underwater time-reversal communication," IEEE J. Oceanic Eng. **41**(3), 644–655 (2016).
[8]B. E. Anderson, M. C. Remillieux, P.-Y. L. Bas, and T. J. Ulrich, "Time reversal techniques," in *Nonlinear Acoustic Techniques for Nondestructive Evaluation*, 1st ed., edited by T. Kundu (Springer and Acoustical Society of America, New York, 2019), pp. 547–581.
[9]S. M. Young, B. E. Anderson, S. M. Hogg, P.-Y. L. Bas, and M. C. Remillieux, "Nonlinearity from stress corrosion cracking as a function of chloride exposure time using the time reversed elastic nonlinearity diagnostic," J. Acoust. Soc. Am. **145**(1), 382–391 (2019).
[10]B. E. Anderson, R. A. Guyer, T. J. Ulrich, and P. A. Johnson, "Time reversal of continuous wave, steady-state signals in elastic media," Appl. Phys. Lett. **94**(11), 111908 (2009).
[11]B. M. Harker and B. E. Anderson, "Optimization of the array mirror for time reversal techniques used in half-space environment," J. Acoust. Soc. Am. **133**, EL351–EL357 (2013).
[12]G. Ribay, J. de Rosny, and M. Fink, "Time reversal of noise sources in a reverberation room," J. Acoust. Soc. Am. **117**(5), 2866–2872 (2005).
[13]R. S. Russell, B. E. Anderson, and M. H. Denison, "Using time reversal with long duration broadband noise signals to achieve high amplitude and a desired spectrum at a target location," Appl. Acoust. **236**, 110744 (2025).
[14]C. Larmat, R. A. Guyer, and P. A. Johnson, "Tremor source location using time-reversal: Selecting the appropriate imaging field," Geophys. Res. Lett. **36**(22), L22304, https://doi.org/10.1029/2009GL040099 (2009).
[15]B. E. Anderson, M. Clemens, and M. L. Willardson, "The effect of transducer directionality on time reversal focusing," J. Acoust. Soc. Am. **142**(1), EL95–EL101 (2017).
[16]S. Yon, M. Tanter, and M. Fink, "Sound focusing in rooms: The time-reversal approach," J. Acoust. Soc. Am. **113**(3), 1533–1543 (2003).
[17]M. H. Denison and B. E. Anderson, "Time reversal acoustics applied to rooms of various reverberation times," J. Acoust. Soc. Am. **144**, 3055–3066 (2018).
[18]M. L. Willardson, B. E. Anderson, S. M. Young, M. H. Denison, and B. D. Patchett, "Time reversal focusing of high amplitude sound in a reverberation chamber," J. Acoust. Soc. Am. **143**(2), 696–705 (2018).
[19]B. D. Patchett and B. E. Anderson, "Nonlinear characteristics of high amplitude focusing using time reversal in a reverberation chamber," J. Acoust. Soc. Am. **151**(6), 3603–3614 (2022).
[20]M. M. Hogg, B. D. Patchett, and B. E. Anderson, "Nonlinear waveform steepening in time reversal focusing of airborne, one-dimensional sound waves," J. Acoust. Soc. Am. **158**(4), 3097–3106 (2025).
[21]M. Farin, C. Prada, and J. de Rosny, "Selective remote excitation of complex structures using time reversal in audible frequency range," J. Acoust. Soc. Am. **146**, 2510–2521 (2019).
[22]M. Farin, C. Prada, T. Lhommeau, M. El Badaoui, and J. de Rosny, "Towards a remote inspection of jet engine blades using time reversal," J. Sound Vib. **525**, 116781 (2022).
[23]M. Tanter, J. Thomas, and M. Fink, "Time reversal and the inverse filter," J. Acoust. Soc. Am. **108**(1), 223–234 (2000).
[24]T. J. Ulrich, B. E. Anderson, P.-Y. L. Bas, C. Payan, J. Douma, and R. Snieder, "Improving time reversal focusing through deconvolution: 20 questions," Proc. Mtgs. Acoust. **16**, 045015 (2012).
[25]B. E. Anderson, J. Douma, T. J. Ulrich, and R. Snieder, "Improving spatio-temporal focusing and source reconstruction through deconvolution," Wave Mot. **52**, 151–159 (2015).
[26]A. D. Kingsley, A. Basham, and B. E. Anderson, "Time reversal imaging of complex sources in a three-dimensional environment using a spatial inverse filter," J. Acoust. Soc. Am. **154**(2), 1018–1027 (2023).
[27]B. E. Anderson, M. Griffa, T. J. Ulrich, and P. A. Johnson, "Time reversal reconstruction of finite sized sources in elastic media," J. Acoust. Soc. Am. **130**(4), EL219–EL225 (2011).
[28]MIL-STD-810G, Department of Defense Test Method Standard, 515.6A-4 (2008).
[29]A. D. Kingsley, J. M. Clift, B. E. Anderson, J. E. Ellsworth, T. J. Ulrich, and P.-Y. L. Bas, "Development of software for performing acoustic time reversal with multiple inputs and outputs," Proc. Mtgs. Acoust. **46**, 055003 (2022).
[30]M. R. Schroeder, "The 'Schroeder frequency' revisited," J. Acoust. Soc Am. **99**(5), 3240–3241 (1996).
[31]ISO 3741:2010, "Sound power and energy in reverberant environments" (International Organization for Standardization, Geneva, Switzerland, 2010).
[32]B. D. Patchett, B. E. Anderson, and A. D. Kingsley, "The impact of room location on time reversal focusing amplitudes," J. Acoust. Soc. Am. **150**(2), 1424–1433 (2021).
[33]D. Cassereau and M. Fink, "Time-reversal of ultrasonic fields: III. Theory of the closed time-reversal cavity," IEEE Trans. Ultrason, Ferroelect, Freq. Contr. **39**(5), 579–592 (1992).